Supporting Information

Multi-functional thermal management for efficient and stable inverted perovskite solar cells

Yongsong Zhang[a], Zhen He[a], Jian Xiong*[a], Shiping Zhan[b], Fu Liu[a], Meng Su[c], Dongjie Wang[a], Yu Huang[a], Qiaogan Liao[a], Jiangrong Lu[a], Zheling Zhang[a], Changlai Yuan[a], Jiang Wang[a], Qilin Dai*[d], and Jian Zhang*[a]

[a] Engineering Research Center of Electronic Information Materials and Devices (Ministry of Education), Guangxi Key Laboratory of Information Materials School of Materials Science and Engineering, Guilin University of Electronic and Technology, Guilin 541004, China

[b] School of Mechatronic Engineering and Automation, Foshan University, Foshan, 528000, P. R. China.

[c] Key Laboratory of Green Printing, Institute of Chemistry Chinese Academy of Sciences (ICCAS), Beijing 100190, P. R. China.

[d] Department of Chemistry, Physics and Atmospheric Sciences Jackson State University Jackson, MS 39217, USA

*Corresponding author e-mail: xiongjian@guet.edu.cn, qilin.dai@jsums.edu, jianzhang@guet.edu.cn.

Supplementary Note S1: First-principles calculations are carried out using the Vienna ab initio simulation package (VASP) code. The projector augmented wave (PAW) method is used to treat the effective interaction of the core electrons and nucleus with the valence electrons, while exchange and correlation are described using the Perdew−Burke−Ernzerhof (PBE) functional. The cut-off energy is set at 400 eV for the plane-wave basis restriction in all calculations. K-points are sampled under the Monkhorst−Pack scheme for the Brillouin-zone integration (K-points are sampled using the Gamma Point). In all calculations, the forces acting on all atoms are < 0.02 eV Å^{-1} in fully relaxed structures, and self-consistency accuracy of 10^{-5} eV is reached for electronic loops.

The method of finite element analysis is used to discuss the mechanism of heat transfer. Finite element simulation without considering surface tension coefficient dependence on temperature. In simulations, the fluid flow is modeled by Navier-Stokes Equation and the solution is treated as incompressible Newtonian Fluid:

$$\rho\left(\frac{\partial u}{\partial t} + u \cdot \nabla u\right) = \nabla \cdot \sigma + F$$

Where ρ is liquid density, u= (u, v) indicates the velocity vector (free movement of liquid induced by temperature difference), t represents the time, σ is liquid Cauchy stress tensor, and F= (0, pg) is the body force. The convection and radiation of heat loss at liquid-air interface can be neglected and heat transfer in liquid domain is governed by:

$$\rho C u \cdot \nabla T = k \nabla^2 T$$

Where C is the heat capacity, T is temperature, k is the thermal conductivity.
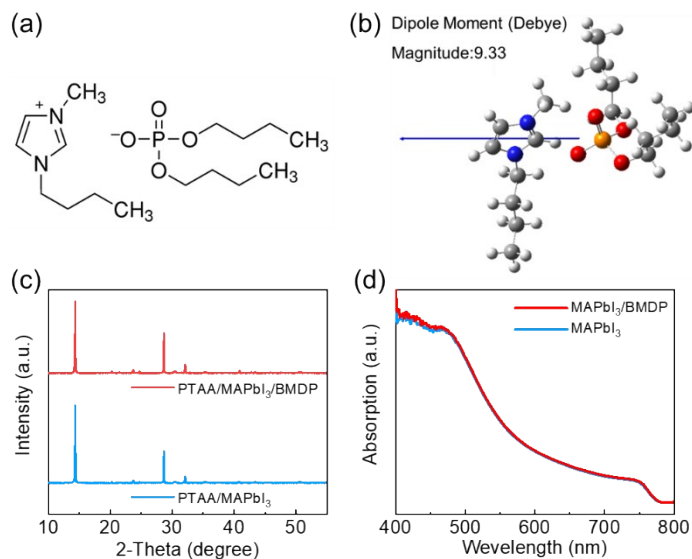
Figure S1. (a) The structural formula of BMDP; (b) Intermolecular dipole moments of BMDP; (c) XRD diffraction patterns of the PTAA/MAPbI$_3$, PTAA/MAPbI$_3$/BMDP films; (d) UV-vis absorption spectra of the MAPbI$_3$, MAPbI$_3$/BMDP films.
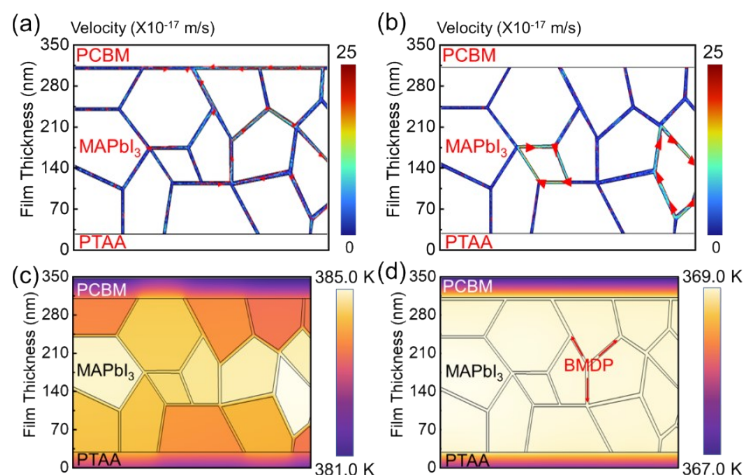

Figure S2. (a) The simulated velocity distribution of BMDP in GBs with a bottom heating power of 0.04 W. (b) The simulated velocity distribution of BMDP in GBs with a heating power of 0.04 W inside perovskite film. (c) and (d) the calculated temperature distribution of ITO/PTAA/MAPbI$_3$/PCBM films without and with BMDP, respectively, with inside heating power of 0.04 W are applied.
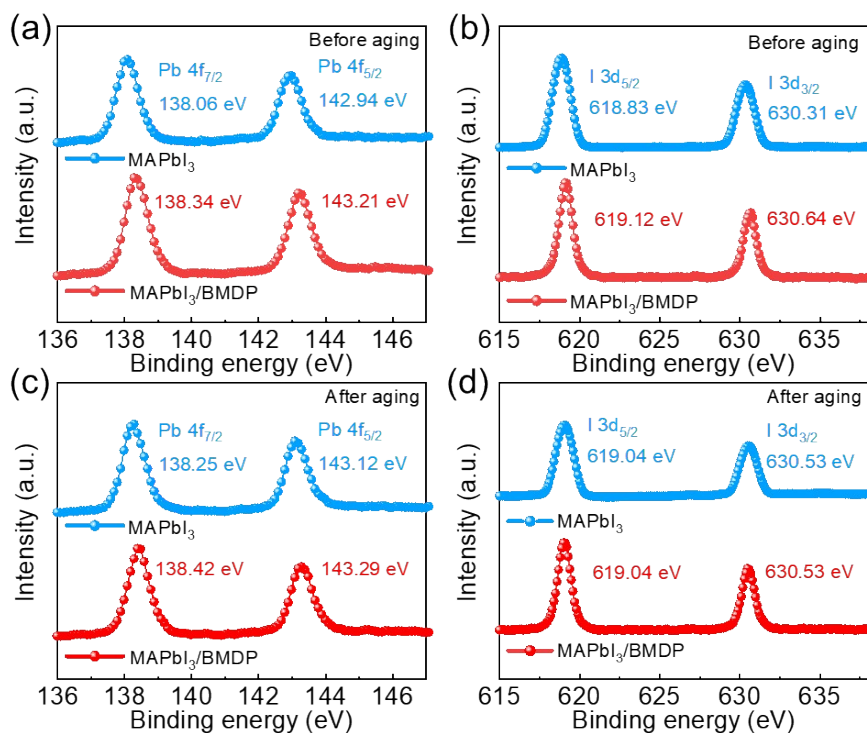
Figure S3. XPS patterns of Pb 4f and I 3d of the different perovskite films before and after thermal aging at 120 ^{o}C for 155 h.
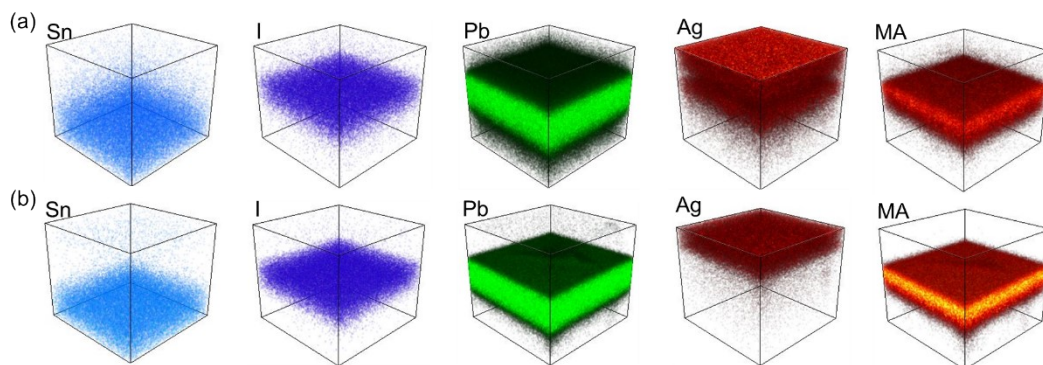
Figure S4. 3D TOF-SIMS for depth profiling of ITO/MAPbI$_3$/PCBM/Ag (a) and ITO/MAPbI$_3$/ BMDP/PCBM/Ag (b) devices after thermal aging at 120°C for 48 h in N$_2$ glove box.
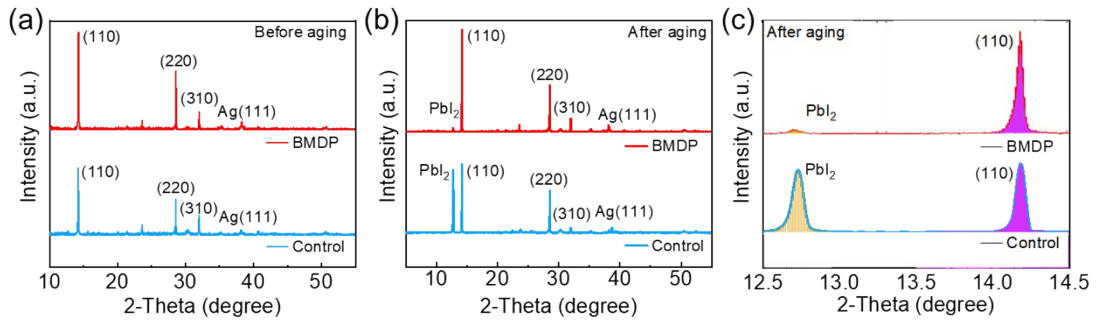
Figure S5. (a) The XRD of the control and BMDP devices before thermal aging; (b) The XRD of the control and BMDP devices after thermal aging at 85 °C for 256 h in N$_2$; (c) The local magnification of XRD spectra in the range of θ=12.5-13.5° of Figure S5b.
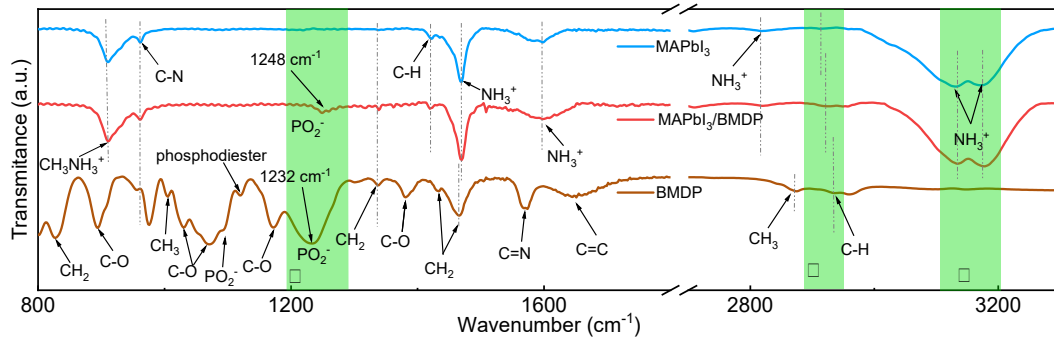
Figure S6. FTIR spectra of the BMDP, MAPbI$_3$, MAPbI$_3$/BMDP samples.
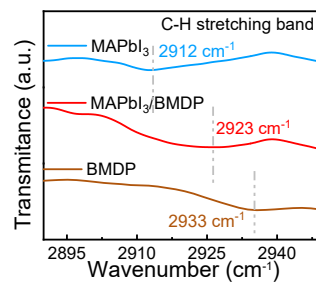
Figure S7. The local magnification of FTIR spectra in the range of 2890-2950 cm^{-1}.
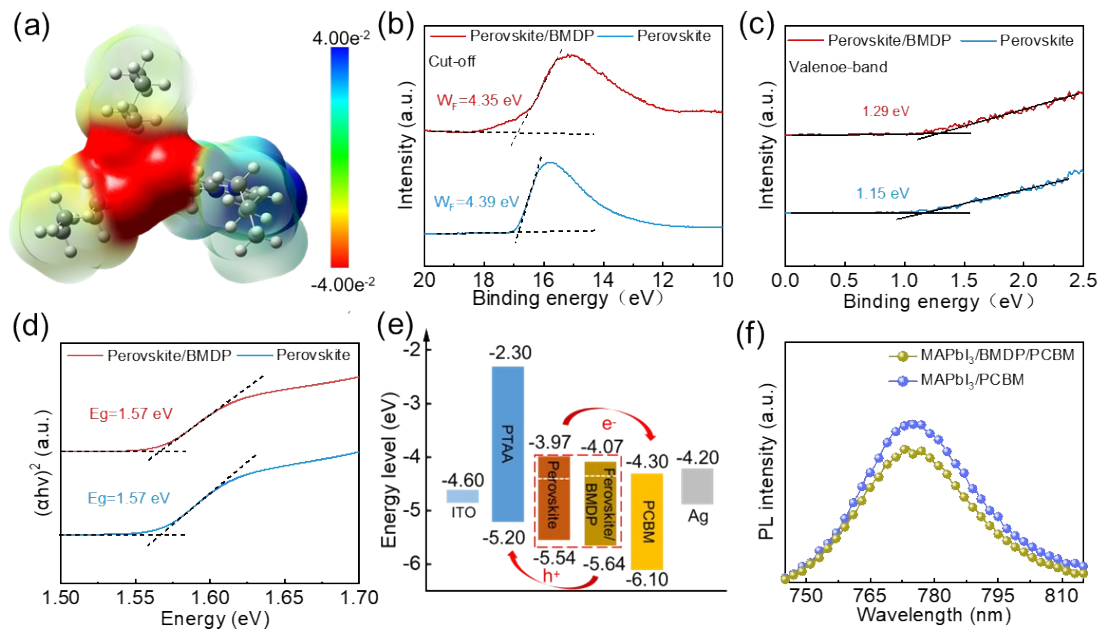
Figure S8. (a) The electrostatic surface potential of BMDP molecular. The UPS secondary electron emission cutoff (b) and valence band edge (c) of the perovskite and perovskite/BMDP films. (d) Tauc plot of perovskite and perovskite/BMDP films. (e) Energy level diagram of the device. (f) The local PL spectra magnification of the region of Figure 4d that labeled by blue circle.
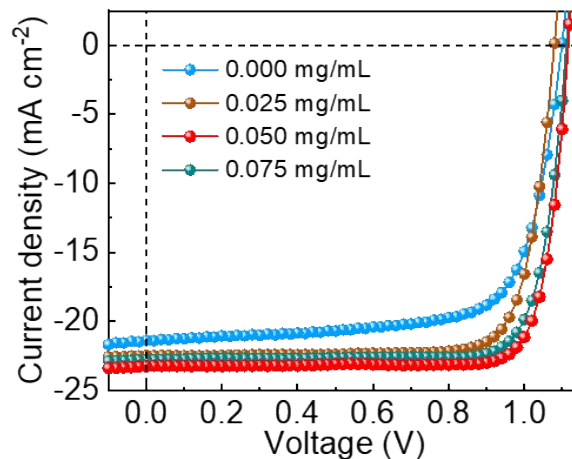
Figure S9. The J-V characteristic curves of the devices with different BMDP concentrations.
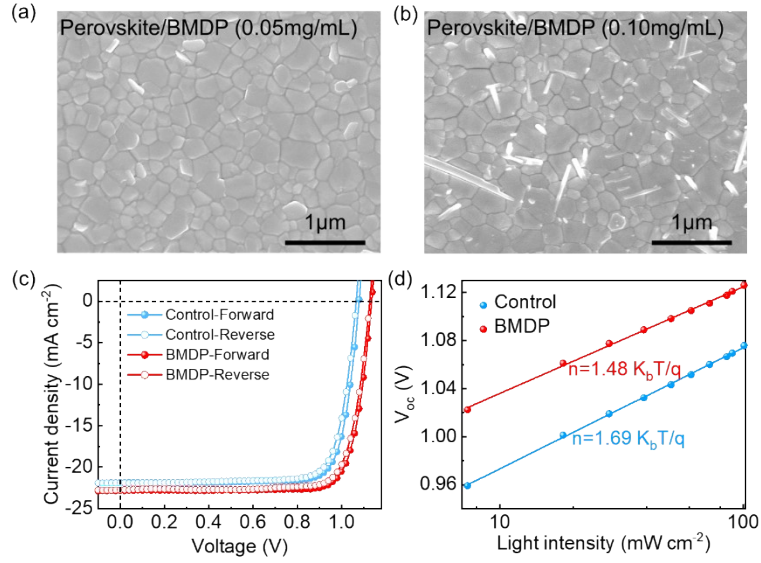
Figure S10 SEM images of BMDP modification with (a) optimal (0.050 mg/mL) and (b) excessive concentration (0.100 mg/mL) (c) The J-V characteristic curves of the control and BMDP devices based on different scan direction. (d) light intensity dependent V_{oc} of the control and BMDP devices.
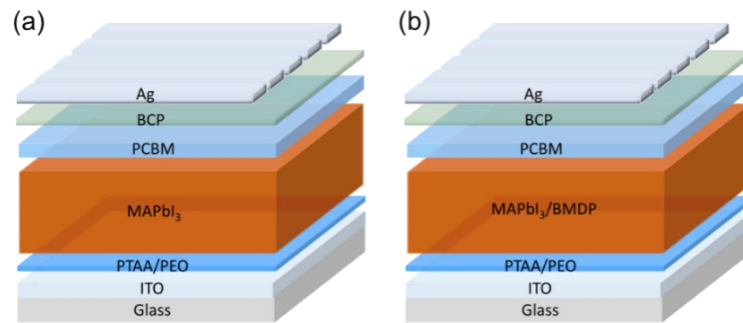
Figure S11. (a) The structure schematic diagram of the PEO device. (b) The structure schematic diagram of the PEO-BMDP device.
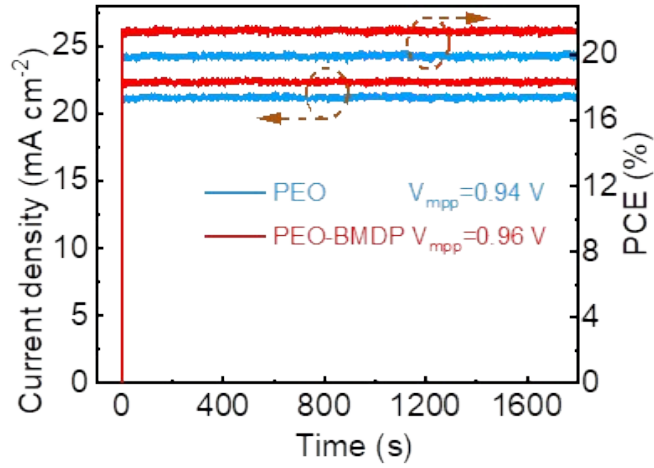
Figure S12. Steady output characteristic of PEO and PEO-BMDP devices.

Table S1. Fitting parameters of the TRPL spectra of the different films.

sample	τ_1 (ns)	A_1	τ_2 (ns)	A_2	τ_{ave} (ns)
MAPbI$_3$	13.96	26.78	30.99	73.22	28.58
MAPbI$_3$/BMDP	12.04	40.36	42.61	59.69	37.71
MAPbI$_3$/PCBM	5.67	99.46	24.24	0.54	6.09
MAPbI$_3$/BMDP/PCBM	5.05	99.75	24.02	0.25	5.28

Table S2. Fitting parameters of the TPV.

sample	τ_1 (ms)	A_1	τ_2 (ms)	A_2	τ_{ave} (ms)
Control	0.28	0	0.05	100	0.05
BMDP	0.44	55.36	1.79	54.64	1.47

Table S3. Fitting parameters of the TPC.

sample	τ_1 (µs)	A_1	τ_2 (µs)	A_2	τ_{ave} (µs)
Control	0.27	18.66	0.27	81.34	0.27
BMDP	0.03	12.39	0.03	87.61	0.03

Table S4. Summary of photovoltaic parameters of the BMDP devices based on different BMDP concentrations. The parameters derived from 15 devices.

BMDP concentration (mg mL^{-1})	V_{OC} (V)	J_{SC} (mA cm^{-2})	FF (%)	PCE (%)
0.000	1.072±0.027 (1.079)	21.95±0.76 (22.48)	78.88±3.30 (80.05)	18.55±1.10 (19.42)
0.025	1.123±0.008 (1.118)	22.22±0.78 (22.22)	79.16±2.43 (81.13)	19.75±0.99 (20.15)
0.050	1.128±0.018 (1.116)	22.73±0.55 (23.28)	80.40±2.66 (82.69)	20.61±1.00 (21.48)
0.075	1.121±0.024 (1.111)	22.38±0.78 (22.81)	78.03±3.59 (81.22)	19.56±1.01 (20.58)

Table S5. The average R_s and R_{sh} of the devices with different BMDP concentrations derived from 16 devices.

Concentration	R_s (Ω)	R_{sh} (Ω)
0.000	149.42	77237.69
0.025	145.66	147195.03
0.050	138.11	182581.34
0.075	149.84	130615.35

Table S6. Performance parameters of the control and BMDP devices based on different scan direction.

Sample	Scan direction	V_{OC} (V)	J_{SC} (mA cm^{-2})	FF (%)	PCE (%)	HI (%)
Control	Forward	1.079	21.83	80.68	19.00	1.60
	Reverse	1.066	21.89	78.90	18.40	
BMDP	Forward	1.136	22.66	81.19	20.83	1.12
	Reverse	1.127	22.52	79.92	20.37	

Table S7. EIS fitting parameters of the control and BMDP devices.

Sample	R_s (Ω)	R_{rec} (Ω)	CPE1 (F)	R_{dr} (Ω)	CPE2 (F)
Control	28.54	8432	4.97×10^{-9}	21436	9.80×10^{-7}
BMDP	6.91	11428	5.05×10^{-9}	79617	8.47×10^{-16}

Table S8. Summary of photovoltaic parameters of the PEO and PEO-BMDP devices. Each parameter is derived from 16 devices.

Sample	V_{OC} (V)	J_{SC} (mA cm^{-2})	FF (%)	PCE (%)
PEO	1.106±0.008 (1.108)	22.50±0.74 (22.64)	79.49±3.18 (81.57)	19.75±0.76 (20.46)
PEO-BMDP	1.123±0.009 (1.132)	23.05±0.52 (23.58)	81.83±1.94 (82.32)	21.19±0.79 (21.98)

Table S9. Literature survey of recent works on the performance of the inverted PSCs based all-solution-processed $MAPbI_3$/PCBM heterojunction.

Device's structure	V_{oc} (V)	J_{sc} (mA cm^{-2})	FF (%)	PCE (%)	Active area (cm^2)	Ref.
ITO/NiO$_x$/MAPbI$_3$/PCBM:PN4N/Ag	1.170	21.80	78.00	19.89	-	[1]
ITO/PTAA-F4TCNQ/PMMA/MAPbI$_3$/ PCBM/Bphen/Al	1.120	23.46	77.50	20.32	0.12	[2]
ITO/NiO$_x$/MAPbI$_3$/PCBM/BCP/Ag	1.110	22.70	78.00	19.54	0.115	[3]
ITO/PTAA/MAPbI$_3$-PCBB-OEG/ PCBM/Al	1.070	23.65	80.00	20.20	-	[4]
ITO/PEDOT:PSS(PEO)/MAPbI$_3$:xNd^{3+} /LiSPS/PCBM/Al	1.040	24.33	83.60	21.15	0.16	[5]
ITO/P3CT-N/MAPbI$_3$/PCBM/BCP/Ag	1.100	22.84	83.17	20.90	0.09	[6]
ITO/PTAA/MAPbI$_3$/PCBB-3N-3I/ PCBM/Al	1.110	23.46	81.36	21.10	0.1	[7]
ITO/PTAA:F4TCNQ/PMMA/MAPbI$_3$/ PCBM/Bphen/Al	1.170	23.79	76.80	21.38	-	[8]
ITO/AI-NiO$_x$/MAPbI$_3$/PCBM/Am- TiO$_x$/Ag	1.060	24.34	81.31	20.84	0.04	[9]
ITO/NiOx/MAPbI$_3$/PCBM/ZrAcac/Ag	1.140	23.28	80.00	21.23	0.04	[10]
ITO/PTAA-F4TCNQ/MAPbI$_3$- capsaicin/PCBM/BCP/Ag	1.130	23.1	83.81	21.88	0.05	[11]
ITO/PTAA/MAPbI$_3$/PCBM/BCP/Ag	1.110	22.74	82.00	21.47	0.04	[12]
ITO/PTAA/MAPbI$_3$-2HT/PCBM/ BCP/Ag	1.080	23.55	80.70	20.61	-	[13]
ITO/PTAA/MAPbI$_3$/4-DA/PCBM-TA/ Ag	1.080	23.29	82.07	20.58	-	[14]
ITO/PTAA/MAPbI$_3$/NBDV/PCBM/ BCP/Ag	1.110	23.82	82.74	21.80	0.04	[15]
ITO/PTAA/MAPbI$_3$/PCBM/OXD- 7/Ag	1.100	23.56	84.63	21.84	0.04	[16]
ITO/PTAA/PEO/MAPbI$_3$/BMDP/ PCBM/Ag	1.132	23.58	82.32	21.98	0.04	This work

Table S10. Summary of photovoltaic parameters of the With or W/O BMDP devices based on different Active layers (parameters derived from 16 devices).

Active layer	Sample	V_{OC} (V)	J_{SC} (mA cm^{-2})	FF (%)	PCE (%)
MAPbI$_3$ (Contain PEO)	W/O BMDP	1.106±0.008 (1.108)	22.50±0.74 (22.64)	79.49±3.18 (81.57)	19.75±0.76 (20.46)
	With BMDP	1.123±0.009 (1.132)	23.05±0.52 (23.58)	81.83±1.94 (82.33)	21.19±0.79 (21.98)
RuCsFAMA	W/O BMDP	1.096±0.027 (1.084)	24.32±0.91 (24.74)	78.69±2.67 (81.36)	20.98±0.95 (21.82)
	With BMDP	1.123±0.016 (1.136)	24.51±0.47 (24.70)	81.22±1.79 (82.85)	22.36±0.89 (23.25)

Table S11. Literature survey of the reports on the thermal stability (85 °C) of the PSCs based on MAPbI$_3$.

Year	Device's structure	Configuration type	Aging time (h)	PCE/PCE$_0$ (%)	Ref.
2018	FTO/bl-TiO$_2$/mp-TiO$_2$/MAPbI$_3$-OA/PTAA/Au	n-i-p	760	80	[17]
2018	FTO/TiO$_2$/MAPbI$_3$-(BA)$_2$(MA)$_{n-1}$Pb$_n$I$_{3n+1}$/Au	n-i-p	720	74	[18]
2019	ITO/PEDOT:PSS/GAMA$_3$Pb$_3$I$_{10}$/PCBM/BCP/Ag	p-i-n	54	50	[19]
2020	FTO/TiO$_2$/MAPbI$_3$/PCBM/Ag	p-i-n	288	94	[20]
2020	FTO/SnO$_2$/MAPbI$_3$/Spiro-OMeTAD/Au	n-i-p	27	85	[21]
2020	ITO/SnO$_2$/Ace$_{0.03}$MA$_{0.97}$PbI$_3$/spiro-MeOTAD/Au	n-i-p	450	92	[22]
2021	ITO/SnO$_2$/MoO$_3$/MAPbI$_3$/spiro-OMeTAD/Au	n-i-p	558	90	[23]
2022	ITO/PTAA/PFN-Br/MAPbI$_3$/PCBM/CzNBr/Cu	p-i-n	1000	80	[24]
2023	ITO/PTAA/MAPbI$_3$/PCBM/RBH/Ag	p-i-n	456	80	[25]
2023	ITO/PTAA/MAPbI$_3$/PCBM/OXD-7/Ag	p-i-n	1080	80	[16]
2023	**ITO/PTAA/MAPbI$_3$/BMDP/PCBM/Ag**	**p-i-n**	**1080**	**88.5**	**This work**

References:

1. Y. Bai, S. Xiao, C. Hu, T. Zhang, X. Meng, H. Lin, Y. Yang and S. Yang, *Adv. Energy Mater.*, 2017, **7**, 1701038.

2. F. Zhang, J. Song, R. Hu, Y. Xiang, J. He, Y. Hao, J. Lian, B. Zhang, P. Zeng and J. Qu, *Small*, 2018, **14**, e1704007.

3. J. Chen, L. Zuo, Y. Zhang, X. Lian, W. Fu, J. Yan, J. Li, G. Wu, C.-Z. Li and H. Chen, *Adv. Energy Mater.*, 2018, **8**, 1800438.

4. G. Xu, R. Xue, W. Chen, J. Zhang, M. Zhang, H. Chen, C. Cui, H. Li, Y. Li and Y. Li, *Adv. Energy Mater.*, 2018, **8**, 1703054.

5. K. Wang, L. Zheng, T. Zhu, X. Yao, C. Yi, X. Zhang, Y. Cao, L. Liu, W. Hu and X. Gong, *Nano Energy*, 2019, **61**, 352-360.

6. Y. Wu, L. Wan, S. Fu, W. Zhang, X. Li and J. Fang, *Journal of Materials Chemistry A*, 2019, **7**, 14136-14144.

7. M. Zhang, Q. Chen, R. Xue, Y. Zhan, C. Wang, J. Lai, J. Yang, H. Lin, J. Yao, Y. Li, L. Chen and Y. Li, *Nat Commun*, 2019, **10**, 4593.

8. F. Zhang, Q. Huang, J. Song, S. Hayase, J. Qu and Q. Shen, *Sol. RRL*, 2020, **4**, 2000149.

9. B. Parida, S. Yoon, J. Ryu, S. Hayase, S. M. Jeong and D.-W. Kang, *ACS Appl. Mater. Interfaces*, 2020, **12**, 22958-22970.

10. Z. W. Gao, Y. Wang, D. Ouyang, H. Liu, Z. Huang, J. Kim and W. C. H. Choy, *Small Methods*, 2020, **4**, 2000478.

11. S. Xiong, Z. Hou, S. Zou, X. Lu, J. Yang, T. Hao, Z. Zhou, J. Xu, Y. Zeng, W. Xiao, W. Dong, D. Li, X. Wang, Z. Hu, L. Sun, Y. Wu, X. Liu, L. Ding, Z. Sun, M. Fahlman and Q. Bao, *Joule*, 2021, **5**, 467-480.

12. J. Xiong, Z. Dai, S. Zhan, X. Zhang, X. Xue, W. Liu, Z. Zhang, Y. Huang, Q. Dai and J. Zhang, *Nano Energy*, 2021, **84**, 105882.

13. F. Li, X. Huang, J. Xue, F. Liu, D. Kim, H.-S. Yang, E. Yang, I. Shin, J. Kim, B. R. Lee and S. H. Park, *Sol. RRL*, 2022, **6**, 2200645.

14. Z. He, J. Xiong, Q. Dai, B. Yang, J. Zhang and S. Xiao, *Nanoscale*, 2020, **12**, 6767-6775.

15. J. Xiong, N. Liu, X. Hu, Y. Qi, W. Liu, J. Dai, Y. Zhang, Z. Dai, X. Zhang, Y. Huang, Z. Zhang, Q. Dai and J. Zhang, *Adv. Energy Mater.*, 2022, **12**, 2201787.

16. N. Liu, J. Xiong, Z. He, C. Yuan, J. Dai, Y. Zhang, C. Zhou, X. Zhang, L. Li, D. Wang, Z. Zhang, Y. Huang, Q. Dai and J. Zhang, *Adv. Energy Mater.*, 2023, **13**, 2300025.

17. M. Jung, T. J. Shin, J. Seo, G. Kim and S. I. Seok, *Energy & Environmental Science*, 2018, **11**, 2188-2197.

18. T. Zhang, M. Long, M. Qin, X. Lu, S. Chen, F. Xie, L. Gong, J. Chen, M. Chu, Q. Miao, Z. Chen, W. Xu, P. Liu, W. Xie and J.-b. Xu, *Joule*, 2018, **2**, 2706-2721.

19. Y. Zhang, J. Chen, X. Lian, W. Yang, J. Li, S. Tian, G. Wu and H. Chen, *Science China Chemistry*, 2019, **62**, 859-865.

20. X. Shi, Y. Wu, J. Chen, M. Cai, Y. Yang, X. Liu, Y. Tao, M. Guli, Y. Ding and S. Dai, *Journal of Materials Chemistry A*, 2020, **8**, 7205-7213.

21. W. Zhang, L. He, D. Tang and X. Li, *Sol. RRL*, 2020, **4**, 2000376.

22. S. Tan, I. Yavuz, N. D. Marco, T. Huang, S.-J. Lee, C. S. Choi, M. Wang, S. Nuryyeva, R. Wang, Y. Zhao, H.-C. Wang, T.-H. Han, B. Dunn, Y. Huang, J.-W. Lee and Y. Yang, *Adv. Mater.*, 2020, **32**, e1906995.

23. C. Liang, H. Gu, Y. Xia, Z. Wang, X. Liu, J. Xia, S. Zuo, Y. Hu, X. Gao, W. Hui, L. Chao, T. Niu, M. Fang, H. Lu, H. Dong, H. Yu, S. Chen, X. Ran, L. Song, B. Li, J. Zhang, Y. Peng, G. Shao, J. Wang, Y. Chen, G. Xing and W. Huang, *Nature Energy*, 2020, **6**, 38-45.

24. Y. R. Kim, J. Kim, H. Kim, H. Back, G. Kim, A. Gu, C.-Y. Nam, J.-H. Kim, H. Suh and K. Lee, *Journal of Materials Chemistry A*, 2022, **10**, 3321-3329.

25. N. Liu, J. Xiong, G. Wang, Z. He, J. Dai, Y. Zhang, Y. Huang, Z. Zhang, D. Wang, S. Li, B. Liu, X. Deng, H. Zhang and J. Zhang, *Adv. Funct. Mater.*, 2023, **33**, 202300396.